

On the Adhesion of Protein in Nitrided Metallic Coatings for Electrosurgical Electrodes of Stainless Steel

R.L. Cruz^a, C.D. Nascimento^a , E.G. Souza^{a*} , C. Aguzzoli^b, A.C.B.K. Moraes^{c,d} , R.G. Lund^d 

^aUniversidade Católica de Pelotas, Mestrado em Engenharia Eletrônica e Computação, 96015-560, Pelotas, RS, Brasil.

^bUniversidade de Caxias do Sul, Departamento de Engenharia de Materiais, 95070-560, Caxias, RS, Brasil.

^cUniversidade Católica de Pelotas, Departamento de Cirurgia Geral, 96015-560, Pelotas, RS, Brasil.

^dUniversidade Federal de Pelotas, Faculdade de Odontologia, Departamento de Odontologia Restauradora, 96010-610, Pelotas, RS, Brasil.

Received: October 20, 2021; Revised: February 02, 2022; Accepted: February 10, 2022.

In this study, it is investigated the anti-adhesive effectiveness of ZrN/Ti and TiN/Ti, deposited by magnetron sputtering, as coating materials of electrosurgical electrodes of steel in protein adhesion tests. Stoichiometry and the thickness of the systems were assessed with Rutherford backscattering spectrometry measurements. Vertical surface deviations were evaluated with the five-point mean height and the arithmetic average height and correlations between the amount of adhered protein in the electrosurgical electrodes and measurements of wettability and electrical resistivity were investigated. The quality of both coatings was put to the test through protein adhesion tests at high temperatures. Cuts with electrosurgical electrodes were performed in an abdominal flap for different electric power and cutting times. The results indicate less adhesion of protein on both proposed coatings, compared to the traditional electrodes of stainless steel, proving to be cheaper alternatives for the surgical industry than other massive anti-adherent electrodes as Au and Ti.

Keywords: *Electrosurgical electrodes, nitride metallic coatings, protein adhesion tests.*

1. Introduction

Electrosurgery, or radio frequency surgery, is a term used to describe a surgical procedure using an electrical current applied to a biological tissue for healing purposes. The surgical benefits are substantial as destroy benign and malignant lesions, cut or excise tissues, and control bleeding¹.

Currently, there are two modalities of electrosurgery, the monopolar and the bipolar. In the monopolar electrosurgery, an active electrode is used to conduct the current to the desired tissue which ends in a return pad. In the bipolar technique, two identical electrodes, similar to a forceps, are used to form a single bipolar instrument and the current only passes through the tissue in the region between the two arms of the forceps².

In both modalities, surgeons have faced many complications as the creation of electric sparks between the forceps tips and, mainly, difficulties with the removal of clots and carbonized tissues as a result of the higher working temperature of the electrodes^{3,4}.

To get around the problem, two ways are reported in the literature, chemical approaches and physical tactics^{5,6}. The physical tactic is related to surface modifications of the electrode, generally by creating micro/nanostructures which reduce the contact area of the electrode with the tissue. However, as reported by Han et al.³, these small

forms can be easily damaged compromising the quality of the electrode in the long term. Alternatively, one could apply a thin-layer coating of an anti-adhesive material to prevent protein adhesion or reducing van der Waals forces⁷.

Some traditional materials have already been tested as electrode constituent materials as Ag, Ti, stainless steel, and Au. The latter showed the best performance, less tendency for adherence of tissue on coagulation and more uniform histological changes on coagulation⁸. However, none of the materials proved to be truly free from sticking. At low powers and short coagulation times, it is hard to see any difference between the amount of coagulum and tissue adhesion. Another issue, especially related to Au, it is the damage to the tips. Any roughness or scratch on the surface of the Au tips could lead to sticking⁹ which makes it the most susceptible to this type of wear. On the face of it, the search for new materials/technologies to coat or manufacture electrodes is still an open challenge.

Transition metals as Ti and Zn are known to be more durable and resistant to corrosion and oxidation than Au, making them good coating materials for stainless steel. Bio-compatibility with human tissue is another remarkable advantage^{10,11}. However, their tribological properties might limit their long-term applications. To improve the wear resistance, zirconium nitride (ZrN) and titanium nitride

*e-mail: everton.granemann@ucpel.edu.br

(TiN), have proved to be good and cheap alternatives to these transition metals.

Some issues also can limit the application of ZrN and TiN coatings as the amount of open porosity between the top layer and the substrate¹². In physical vapor deposition (PVD) techniques, as DC-Magnetron sputtering, defects such as voids, pinholes, pores, cracks, and even delamination cannot be completely ruled out, and the open paths between the substrate and the corrosive environment could compromise the durability of the electrodes¹³. As a solution, some authors proposed the deposition of an interlayer between the substrate and the top layer¹⁴, forming a multilayer system.

The success of multilayer adhesion strongly depends on the selection of a suitable pair of materials. There are numerous possibilities in the literature, and the choice depends on the property one wishes to obtain¹⁵⁻²⁰. If one would like to decrease the adhesion of fluids and increase the corrosion resistance of the electrode tips, TiN and ZrN might be good choices. However, TiN and ZrN alone are hard and brittle coatings and a combination with a softer metal in the interlayer, such as Ti, is recommended to manage interfacial stress and to arrest crack growth^{21,22}. The effectiveness of Ti as interlayer of ZrN and TiN has also been documented in simulations involving pseudo-potentials and density functional theory (DFT), in a recent work published by Zavodinsky and Kabaldin²³.

Motivated by the difficulties faced by surgeons with the removal of carbonized tissues adhered to electro-surgical electrodes, in this study, it is proposed the application of TiN/Ti and ZrN/Ti as coating materials of electrodes of stainless steel (AISI 302). Most studies found in literature deals with the adhesion of platelets and proteins at room temperature, without check performance at higher temperatures, similar to the one experienced by surgeons in a real environment²⁴⁻²⁷. Particularly, for the electro-surgical electrodes, it was found only one study⁸ correlating morphological and structural properties of the constituent materials of the electrode to protein adhesion tests. Although this related work is a relevant scientific contribution, the findings are limited to the use of classical materials of commercial electrodes as Au, Ti, and steel, and no alternative material is proposed for new industrial applications. In addition, the experimental adhesion tests proposed here are performed in a human abdominal flap instead of the femoral arteries of Wistar rats.

To carry on the analyzes proposed here, rectangular thin films systems of TiN/Ti and ZrN/Ti were previously prepared for different deposition temperatures of the Ti interlayer to verify the influence of this parameter on the rugosity, wettability, and electrical resistivity as well as to correlate with the protein adhesion to the electro-surgical electrodes.

Then, commercial electro-surgical electrodes of stainless steel (AISI 302) were coated with layers of TiN/Ti and ZrN/Ti, in similar conditions of the thin film systems. The effectiveness of the nitrided coated electrodes was compared with stainless steel electrodes in protein adhesion tests. The tests were performed by cutting a human abdominal flap for different electric power and cutting times, well discussed in the last section of the manuscript.

2. Materials and Methods

ZrN and TiN thin films with a buffer interlayer of Ti were deposited on substrates of C (Carbono Lorena Ltda) and stainless steel (AISI 302) by using a magnetron sputtering. Prior to deposition, all substrates were cleaned by ultrasonic acetone bath and immediately loaded in the sputtering vacuum chamber, which was pumped down to a base pressure of 5.0×10^{-5} Pa. The targets were sputtered 6.0 cm away from the substrates which were at a bias voltage of -150 V. Also, an input DC power of 100 W was employed to the Ti interlayer and the ZrN top layer. For TiN, 70 W of RF power was used. The ZrN coating was generated with reactive magnetron sputtering while the TiN coating was made from a target of this material.

To investigate the influence of the temperature on properties of the systems, the deposition of the Ti interlayer was carried out at temperatures of 100°, 200° and 300° C. To get a better stoichiometry, the top layers were deposited at different temperatures, 400°C for ZrN and 100°C for TiN. The depositions were performed by using Ar as an inert gas, with a constant partial pressure of 5.0×10^{-1} Pa. The deposition times for each layer were 30 min for TiN, 15 min for ZrN, and 1 min for the interlayer of Ti.

To determine the wettability of the samples, the sessile drop technique was employed by using a goniometer Model 300, SEO Phoenix, South Korea. For each sample, three drops of distilled water in the micrometer scale were created, and for each drop, ten measurements were performed.

Surface roughness was measured using a Taylor Hobson device, model 112/2009 with a tip radius of 2 μm and a cone angle of 90°. To improve the reliability of the results, the five-point mean roughness profile (R_z) was measured in three distinct regions of the samples and the results were expressed in terms of the averages and the standard deviation. The electrical resistivity was determined with the sheet resistance method by using an in-line four-point probe device with tungsten tips. The equipment was connected to a current source, operating at 20 mA, and the sample voltage was measured with a 5.5 digit multimeter. All the measurements were performed in the center of the samples, repeated five times, and expressed in terms of averages and the standard deviations. The Rutherford Backscattering Spectrometry (RBS) was performed with a 2 MeV He^+ ion impinging along the normal surface of the samples with a scattered angle of 165°. The accuracy of the energy peaks, i.e. a channel to energy conversion, was obtained from a calibration curve with heavy elements^{28,29}. In order to avoid a mixture of peaks and low count of certain elements, substrates of C were preferred for RBS. For surface roughness, wettability, and electrical resistivity substrates, steel and C, were preferred due to the little influence of them in these superficial measurements.

In protein adhesion tests, three commercial stainless steel monopolar knife straight electrodes, with 2.38 mm-wide tips (model EF21, WEM), were connected to the electro-surgical unit (EMAI Model BP-150). Then, two electrodes were coated, following similar deposition procedures used for the thin film systems, with bi-layers of TiN/Ti and ZrN/Ti. For both electrodes, it was adopted an interlayer thickness of ~15 nm and top layers thickness of 80 nm for TiN and 150 nm for ZrN. Before the depositions, both electrodes

were submitted to a physical etch attack with atoms of Ar³⁰, in order to remove the impurities and improve the adhesion of the coating layers to the substrate. To remove undesired substances before each surgical procedure (cut), the electrodes were washed with deionized water and then, carefully dried. Then, the amount of protein during the adhesion tests was measured from the difference in weight of each electrode before and after a cut with an analytical balance (Shimadzu, ATY224) with a resolution of 0.0001 g.

3. Results and Discussion

3.1. Stoichiometry and sample thickness

Figure 1 shows the composition results obtained from RBS measurements for ZrN/Ti, and TiN/Ti as a function of the deposition temperature of the interlayer of Ti. The experimental RBS spectra are depicted as black dots with the arrows indicating the location of each element. The area under the curves is filled to highlight the visualization of the data.

The left side of Figure 1, frames (a), (b), and (c), shows a similar energy range for Zr (1600–1700 keV) and N (575–630 keV) for all the deposition temperatures of the interlayer. This result indicates a similar thickness of the elements of the top layer (ZrN) and little influence of the deposition temperature in the manufacturing process.

Also in Figure 1, it is remarkable that the Ti signal on the left side is less prominent than on the right side, indicating a lower concentration of Ti in ZrN/Ti than in TiN/Ti. This is because, differently of ZrN/Ti, TiN/Ti has Ti in both the interlayer and the top layer.

The full width at half maximum (FWHM) of each element peak is proportional to the product of the stopping power factor and the thickness of each element³¹. Thus, to estimate the thickness of the layers and the chemical composition of the elements, a simulation over the experimental RBS spectra was carried out using the SIMNRA software³². The results of the simulations are depicted in Figure 1 as full red lines. The estimated thickness and the chemical compositions of the top layer and the interlayer, as a function of deposition temperature of Ti, are displayed in Table 1.

As one can see, the interlayer of ZrN/Ti and TiN/Ti leads to about the same thickness, but with a discrepancy in the top layer. Following the arguments of Vega et al.¹², TiN/Ti could improve its resistance to corrosion when there is a similar proportion of material between the interlayer and the top layer. On the other hand, better results are obtained when the top layer of ZrN/Ti is thick enough and tight³³.

To allow a deeper analysis of the origin of the O contamination, the percentage values exhibited in Table 1 were calculated independently for each layer. As one can

Table 1. Thickness and composition of systems layers obtained by SIMNRA simulations. The uncertainties associated with the thicknesses values are not greater than 5%.

Sample - Temperature (°C)	Top Layer					Interlayer		
	Thickness (nm)	% N (at)	% Ti (at)	% Zr (at)	% O (at)	Thickness (nm)	% Ti (at)	% O (at)
ZrN/Ti - 100	121.0	43.5	-	47.5	9.0	21.0	90.0	10.0
ZrN/Ti - 200	116.0	40.0	-	50.0	10.0	22.0	90.0	10.0
ZrN/Ti - 300	138.0	40.0	-	50.0	10.0	21.0	90.0	10.0
TiN/Ti - 100	10.0	47.0	47.0	-	6.0	14.0	78.0	22.0
TiN/Ti - 200	10.0	47.0	47.0	-	6.0	13.0	85.0	15.0
TiN/Ti - 300	11.0	46.0	46.0	-	8.0	12.0	80.0	20.0

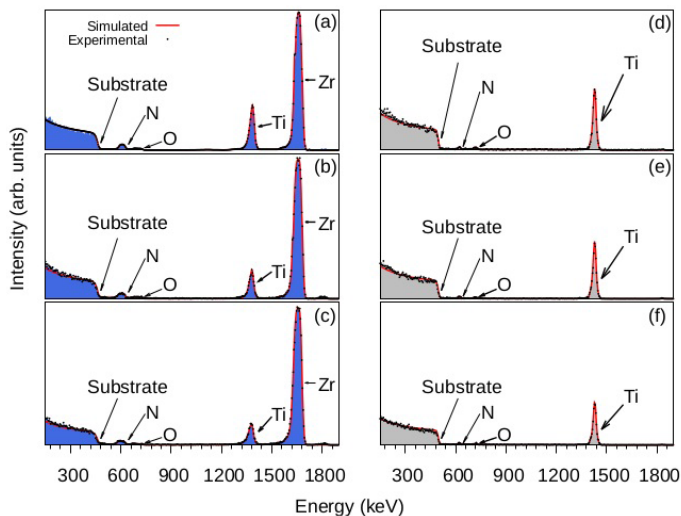


Figure 1. RBS measurements of ZrN/Ti (left) and TiN/Ti (right) systems deposited on C substrate for three different interlayer temperatures. For labels (a) and (d) T = 100°C, (b) and (e) T = 200°C, and (c) and (f) T = 300°C. The arrows indicate the surface energy, the black dots the experimental data, and the SIMNRA simulations are depicted as full red lines.

see, O represents, by averaging the temperature values of T_p , $\sim 10.0\%$ and $\sim 19\%$ of the composition of the adhesion layer of ZrN/Ti and TiN/Ti, respectively. Due to the location of O in the interlayer, we believe that the source of oxidation is due to its presence of oxygen and water vapor from the plasma chamber walls and/or due to small leaks on the system.

As an example of the calculations displayed in Table 1, one can consider the percentage of both, the interlayer and the top layer, the portion of O would represent a small part of the total chemical composition of the system. For an isotropic distribution composed of all the chemical elements in the system, one could estimate the average amount of O by applying a weighted average. Then, the weighting factor (w_i) should be the ratio between the thickness of each layer and the total thickness of the system. For instance, for ZrN/Ti at 100°C , we could find the weighting factors: $w_1 = 121/142$ for the top layer and $w_2 = 21/142$ for the interlayer. Thus, the average amount of O in this sample should be:

$$\bar{O} = \frac{121}{142}(0.09) + \frac{21}{142}(0.10) = \frac{1299}{14200} \approx 0.091 = 9.2\%$$

Where the values, 0.09 and 0.01, are the percentage of O in the top layer and the interlayer, respectively.

3.2. Roughness, wettability, and electrical conductivity

To assess the degree of unevenness of the systems surface, the mean roughness profile depth (R_z) and the arithmetic average height (R_a) of each system group, and also for a reference substrate of steel, was evaluated with profilometry measurements³⁴. The results are shown in Table 2 as a function of the interlayer deposition temperature.

As one can see, the surface roughness of all the systems is comparable, if one takes into account the standard deviation of the measurements. The systems also present statistical similarities regarding the average peak-valley height, indicating little or no gain in roughness after coating. According to Jacobson et. al.³⁵, systems with similar roughness values resemble also in wear resistance.

Figure 2 shows the wettability measurements for both nitrided samples and stainless steel. Steel is represented by dashed lines because it is a pure sample, without an interlayer, and therefore independent of the deposition temperature. As one could see, all the systems exhibit contact angles smaller than 90° and thus a hydrophilic behavior, but the degree of

Table 2. Results from the profilometry analysis. The amplitude parameter R_z represents the mean roughness profile depth while R_a is the arithmetic average height. The label “Steel” represents the results of the commercial electro-surgical electrode (AISI 302).

Sample - Temp ($^\circ\text{C}$)	R_a (nm)	R_z (nm)
ZrN/Ti - 100	35 ± 2	256 ± 24
ZrN/Ti - 200	37 ± 2	285 ± 24
ZrN/Ti - 300	32 ± 1	233 ± 34
TiN/Ti - 100	35 ± 4	290 ± 59
TiN/Ti - 200	36 ± 7	254 ± 72
TiN/Ti - 300	34 ± 2	237 ± 32
Steel - Room Temp.	34 ± 6	235 ± 57

hydrophilicity is different as the deposition temperature of the interlayer changes. For ZrN/Ti, the contact angle ranges from 76.5° to 64° . Statistically, for 100° and 200°C , ZrN/Ti showed an equivalent wettability and the more hydrophobic (closer to 90° angle) behavior between the analyzed samples. TiN/Ti is the most hydrophilic alloy with contact angles ranging in between 53.0° to 62.0° , showing the most near hydrophobic behavior at the deposition temperature of $T = 200^\circ\text{C}$. This dependence of the wettability with the temperature was observed in the studies of Sun et al.³⁶ for single layers of TiN and ZrN. However, their studies were performed with a variation of the surface temperature and not the deposition temperature of the buffer layer.

The change in the nitrided coatings nanostructures due to the presence of the interlayer has a direct effect on macroscopic properties, such as electrical resistivity. In the case of an equally spaced in-line four-point probe geometry the resistivity, ρ , could be calculated using the infinite 2D sheet approach³⁷, $\rho = f.t.R_{sh}$, where $R_{sh} = V/I$ is the sheet resistance, $f = \pi/\ln 2$ is the geometric factor and t is the system thickness. The results are depicted in Figure 3.

As the sample of steel was measured only at room temperature with no deposition, it is represented by a dashed line for all the temperature values due to the nonexistence of the interlayer.

The samples of TiN/Ti show a decrease in electrical resistivity with an increase in the deposition temperature of the interlayer. This behavior had already been reported by Tsai et al.³⁸ for monolayers of TiN. According to them, this improvement in electrical resistivity is attributed to an increase in the densities of thin films. We believe that a similar mechanism is responsible for the increase in the electrical conductivity of TiN/Ti since all the systems at these temperatures have an equivalent surface roughness (Table 2) and a similar amount of O (Table 1). ZrN/Ti presents higher electrical resistivity than TiN/Ti and a constant electrical resistivity as the deposition temperature changes. The thickness of the ZrN/Ti systems is undoubtedly one of the main reasons for this unexpected behavior since ZrN possesses the lowest electrical resistivity in bulk among all the transition-metal oxides³⁹.

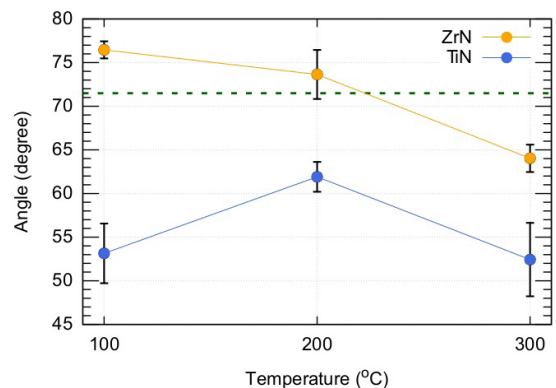


Figure 2. Wettability measures as a function of the deposition temperature of Ti. The results are averages over ten measurements. The bar indicates the uncertainty associated with each measurement.

3.3. Experimental results with electrosurgical electrodes

In order to correlate the results obtained for the systems of thin films, protein adhesion tests were performed with electrosurgical electrodes of stainless steel. Two of them were coated with bi-layers of TiN/Ti and ZrN/Ti, respectively, and another one, of stainless steel, was used as a reference electrode for comparisons. Aiming industrial applications, the lowest temperature, 100° C, was chosen for the deposition of the interlayer of Ti. The appearance of the electrodes after

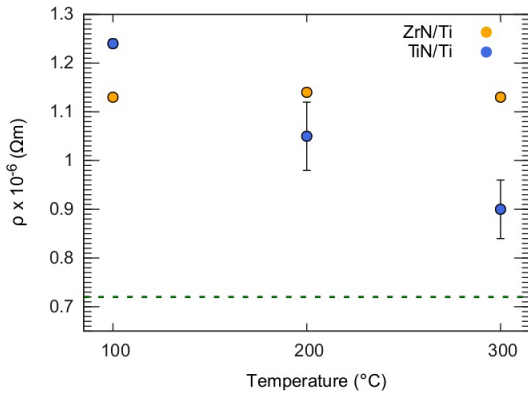


Figure 3. Electrical resistivity measurements, ρ , for different deposition temperatures of the Ti interlayer. These results are averages over five different central measurements, all of them performed on a squared thin film with surface area of $\sim 1.0 \text{ cm}^2$. The uncertainties for ZrN are not displayed ($\sim 0.5\%$, for all samples) because they are smaller than the symbols. The steel is represented by dashed lines.

the deposition process as well as the reference electrode is shown in Figure 4a with labels (1), (2) and (3).

To perform the tests and obtain little hemostasis, the electrosurgical unit was adjusted to the pure cutting function. Every cut was performed in an abdominal flap, legally acquired with approved and recognized procedures, of 42.0 cm x 17.4 cm size (Figure 4b) maintaining the same depth and incision angle ($\sim 35^\circ$), in a procedure similar with that used by Mikami⁸.

The amount of adhered protein was measured by the difference in weight of each electrode before and after a cut. Due to the sensitivity of the analytical balance, every cut was weighted three times, obtaining an average weight per cut. In addition to this procedure, the cuts were repeated two times to reduce experimental errors. Figure 4c shows the wear the electrodes after the whole experimental section. Figure 5 displayed the results for different incision times (4s, 7s and 10s) and electric power.

The electric power in the x-axis has a nonlinear relationship with the real power provided by the electrosurgical unit. The conversion depends on the impedance and the electrical conductivity of the tissue being cut. According to the manufacturer's manual⁴⁰, if one considers a tissue impedance of 300 Ω , the power scales 3, 5, and 7 would correspond to the real power values of 139.33 W, 255.5 W, and 312.94 W, respectively.

In general, the experiment shows consistent results with what is expected, the greater the power and the cutting time, the greater the protein adhesion on the tips of the electrodes. Exceptions are found for steel in power scale 3 and cutting times of 4s and 7s (first point in Figure 5a and 5b) where steel shows a similar adhesion of proteins. ZrN/Ti also exhibits

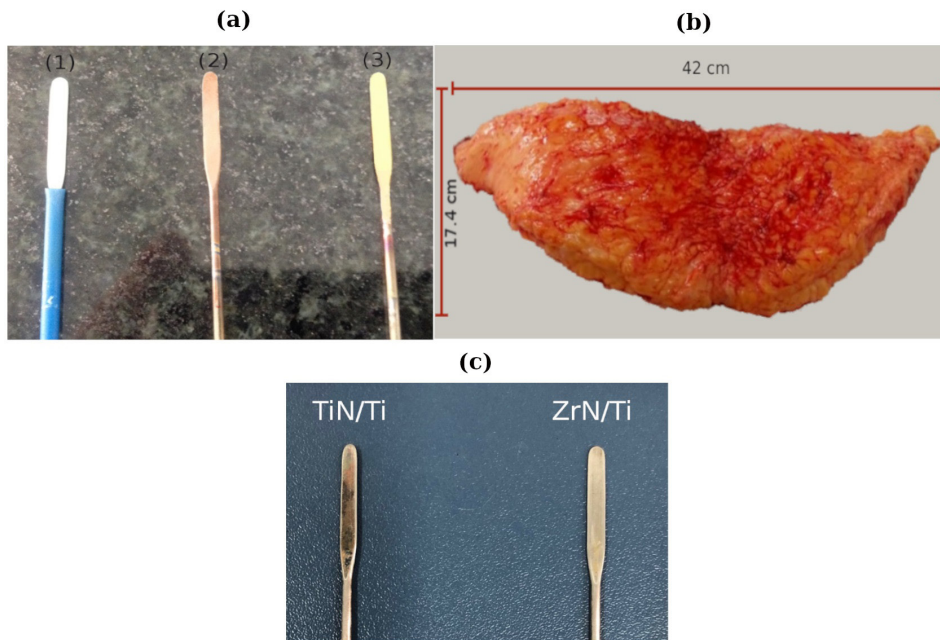


Figure 4. Frame (a) shows the electrosurgical electrodes used during the protein adhesion tests. Label (1) represents the stainless steel electrode with no coating. Labels (2) and (3) represent the coated electrodes with TiN/Ti and ZrN/Ti layers, respectively, right after the deposition process. The frame (b) displays the human abdominal flap used during the adhesion tests. The frame (c) shows the wear of the electrodes at the end of the experiment.

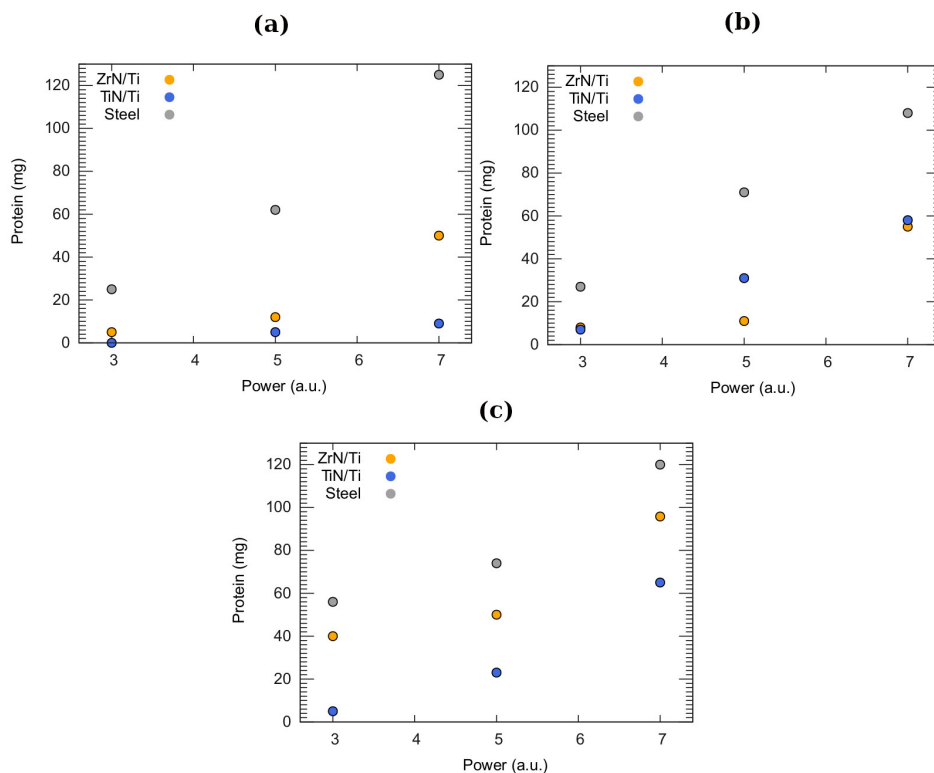


Figure 5. Protein adhesion tests for different cutting times and equipment power. The frames (a), (b), and (c) represent the cutting times for 4s, 7s, and 10s, respectively. The maximum dispersion in the measurements is smaller than 15 mg of protein.

an unexpected behavior with similar protein adhesion for powers 3 and 5 in Figure 5b.

Regardless of the cutting time and electric power, the reference electrode of steel showed lower performance than the coated electrodes in all the adhesion tests. Further, coated electrodes exhibited, statistically, similar adhesion of protein for cutting times of 4s and 7s (Figures 5a and 5b). As the whole experiment was performed in a single experimental section, from the lowest to the highest cutting time, it was expected more intense wear of the coating at 10s (Figure 5c). This effect is perceived for ZrN/Ti, in Figure 5c, which decreases its relative performance with respect to TiN/Ti (showed in Figures 5a and 5b) reaching levels of protein adhesion closer to stainless steel. It is believed that the durability of the coating is related to the choice of the coating and the interlayer materials, as TiN bonds more easily with the interlayer of Ti than ZrN.

In addition, TiN/Ti, the most hydrophilic material according to Figure 2, seems to promote the lowest level of protein adhesion. The adhesion in the electrodes of TiN/Ti was lower than ZrN/Ti for 4s (Figure 5a), similar for 7s (Figure 5b), and lower again for 10s, especially due to the mixture with the wear effects in the electrodes of ZrN/Ti. This result is somehow related to the studies documented by Jones et al.²⁴. In analyzes of protein adsorption on discs of TiN, they found that the most hydrophilic surfaces did appear to promote greater amounts of fibrinogen adsorption.

Comparing the electrical conductivity of the samples (Figure 3) for all the scenarios of Figure 5, stainless steel

presented the better electrical conductivity but the higher adhesion of protein. Similarly, TiN/Ti showed the lower electrical conductivity among the analyzed samples, however, it had the better performance for short and long cutting times (Figures 5a and 5c) and a similar protein adhesion for intermediate cutting times (Figures 5b and 5c). ZrN/Ti presented a proportional relationship between electrical conductivity and protein adhesion for short cutting times, however, this behavior was not sustained for longer cutting times. On the face of it, no clear relationship between electrical resistivity and protein adhesion on the electrodes could be determined.

According to Figure 1, the surface roughness of electrodes is similar, which results in comparable friction for coated and uncoated electrodes. Nevertheless, ceramic materials such as ZrN and TiN have greater electronegativity, that is, they do not lose electrons as easily compared to materials with metallic properties such as those that make up AISI 302 like Fe, Cr, and Ni alloys⁴¹. This greater electronegativity is due to the stability of these transition metal nitrides in the valence layer which protect the coated electrodes of stainless steel reducing the loss of electrons to oxygen molecules. Some studies indicate that when the oxides present in the surface of steel interact with proteins, there is an enrichment of the chromium oxide⁴², one of the main responsible to prevent the oxidation of the stainless steel. This effect is related to the protein-induced metal release, in corrosion processes, and also with the increase of the adhesion of proteins, which

is believed to be the main response to the higher adhesion of protein to the stainless steel electrodes.

4. Conclusions

In this work, it was compared the performance of ZrN/Ti and TiN/Ti, as coating materials of electrosurgical electrodes of steel, with non-coated electrodes of stainless steel. The analyses were carried out using thin film systems and coated electrosurgical electrodes deposited under similar conditions by magnetron sputtering.

Stoichiometry results, obtained from RBS measurements and SIMNRA simulations, showed a presence of oxygen between 6 to 10% during the deposition process. Profilometry analyzes indicated samples with equivalent rugosity with a non-significant dependence of the interlayer deposition temperature. In contrast, the wettability and the electrical resistivity measurements showed a temperature-dependent character.

The adhesion tests in the abdominal flap showed no direct relationship between the electrical resistivity and protein adhesion on the electrosurgical electrodes.

Since the rugosity of ZrN/Ti, TiN/Ti, and stainless steel electrodes were similar, the little affinity for oxygen atoms of both nitrided coatings promoted a lower adhesion of protein to their surface than to stainless steel.

All samples showed hydrophilic properties, with higher contact angles of ZrN/Ti than TiN/Ti for all the interlayer temperatures tested. Nevertheless, the most hydrophilic material, ZrN/Ti, presented the lowest level of protein adhesion.

5. Acknowledgments

This work was partially supported by FAPERGS, Brazil, under grant number 17/2551-0000808-1 (ARD). It was developed in collaboration with the Ion Implantation Laboratory and the Microelectronics Laboratory of the Institute of Physics of the Federal University of Rio Grande do Sul, Porto Alegre, RS, Brazil. The authors declare no conflict of interest regarding the publication of this article.

6. References

- Hainer BL, Usatine RB. Electrosurgery for skin. *Am Fam Physician*. 2002;66:1259-67.
- Afonso CT, Silva AL, Fabrini DS, Afonso CT, Côrtes MGW, Sant'Anna LL. Risk of the use of electrocautery in patient with metallic ornaments. *Arq Bras Cir Dig*. 2010;23(3):183-6.
- Han Z, Fu J, Feng X, Niu S, Rena L. Bionic anti-adhesive electrode coupled with maize leaf microstructures and TiO₂ coating. *RSC Adv*. 2017;7:45287-93.
- Elliott-Lewis EW, Mason AM, Barrow DL. Evaluation of a new bipolar coagulation forceps in a thermal damage assessment. *Neurosurg*. 2019;65(6):1182-7.
- Sotiri I, Overton JC, Waterhouse A, Howell C. Immobilized liquid layers: a new approach to anti-adhesion surfaces for medical applications. *Exp Biol Med*. 2016;241(9):909-18.
- Banerjee I, Pangule RC, Kane RS. Antifouling coatings: recent developments in the design of surfaces that prevent fouling by proteins, bacteria, and marine organisms. *Adv Mater*. 2011;23(6):690-718.
- Ebnesajjad S, editor. *Fluoroplastics: non-melt processible uoroplastics*. USA: Elsevier; 2000. (vol. 1).
- Mikami T, Takahashi A, Hashi K, Gasa S, Houkin K. Performance of bipolar forceps during coagulation and its dependence on the tip material: a quantitative experimental assay. *J Neurosurg*. 2004;100(1):133-8.
- Menovsky T. Bipolar forceps. *J Neurosurg*. 2004;101(6):1082-3.
- Okazaki Y, Ito Y, Kyo K, Tateishi T. Corrosion resistance and corrosion fatigue strength of new titanium alloys for medical implants without V and Al. *Mater Sci Eng A*. 1996;213(1-2):138-47.
- Davidson JA, Mishra AK, Kovacs P, Poggie RA. New surface-hardened, low-modulus, corrosion-resistant Ti-13Nb-13Zr alloy for total HIP arthroplasty. *Biomed Mater Eng*. 1994;131(3):231-43.
- Vega J, Scheerer H, Andersohn G, Oechsner M. Experimental studies of the effect of Ti interlayers on the corrosion resistance of TiN PVD coatings by using electrochemical methods. *Corros Sci*. 2018;133:240-50.
- Lin SS, Zhou KS, Dai MJ, Hu F, Shi Q, Hou HJ, et al. Effects of surface roughness of substrate on properties of Ti/TiN/Zr/ZrN multilayer coatings. *Trans Nonferrous Met Soc China*. 2015;25(2):451-6.
- Wan Q, Ding H, Yousaf MI, Chen YM, Liu HD, Hu L, et al. Corrosion behaviors of TiN and Ti-Si-N (with 2.9at.% and 5.0at.%Si) coatings by electrochemical impedance spectroscopy. *Thin Solid Films*. 2016;616:601-7.
- Li D, Chu X, Cheng SC, Lin XW, Dravid VP, Chung YW, et al. Synthesis of superhard carbon nitride composite coatings. *Appl Phys Lett*. 1995;67:203-5.
- Chu X, Wong MS, Sproul WD, Barnett SA. Mechanical properties and microstructures of polycrystalline ceramic/metal superlattices: TiN/Ni and TiN/Ni_{0.9}Cr_{0.1}. *Surf Coat Tech*. 1993;61(1-3):251-6.
- He JL, Li WZ, Li HD. Simulation of nacre with TiN/Pt multilayers and a study of their hardness. *J Mater Res*. 1997;12(11):3140-5.
- Abadias G, Tse YY, Michel A, Jaouen C, Jaouen M. Nanoscaled composite TiN/Cu multilayer thin films deposited by dual ion beam sputtering: growth and structural characterization. *Thin Solid Films*. 2003;433(166):166-73.
- Wu ML, Qian WD, Chung YW, Wang YY, Wong MS, Sproul WD. Superhard coatings of CN_x/ZrN multilayers prepared by DC magnetron sputtering. *Thin Solid Films*. 1997;308:113-7.
- Junhua X, Geyang L, Mingyuan G. The microstructure and mechanical properties of TaN/TiN and TaWN/TiN superlattice films. *Thin Solid Films*. 2000;370(1-2):45-9.
- Ziebert C, Ulrich S. Hard multilayer coatings containing TiN and/or ZrN: a review and recent progress in their nanoscale characterization. *J Vac Sci Technol A*. 2006;24(554):554-83.
- Nascimento CD, Souza EG, Aguzzoli C, Cruz RL. Effects of oxygen on the resistivity in Au thin films with Ti-Al adhesion layer. *J Vac Sci Technol B*. 2019;37(5):052202.
- Zavodinsky VG, Kabaldin YG. Adhesion and mechanical properties of layered nano films TiN/ZrN and TiN/Ti/ZrN: pseudopotential simulation. *Compos Interfaces*. 2019;26(2):97-106.
- Jones MI, McColl IR, Grant DM, Parker KG, Parker TL. Protein adsorption and platelet attachment and activation, on TiN, TiC, and DLC coatings on titanium for cardiovascular applications. *J Biomed Mater Res*. 2000;52(2):413-21.
- Manzi BM, Werner M, Ivanova EP, Crawford RJ, Baulin VA. Simulations of protein adsorption on nanostructured surfaces. *Sci Rep*. 2019;9(1):4694.
- Maddikeri RR, Tosatti S, Schuler M, Chessari S, Textor M, Richards RG, et al. Reduced medical infection related bacterial strains adhesion on bioactive RGD modified titanium surfaces: a first step toward cell selective surfaces. *J Biomed Mater Res A*. 2007;84A(2):425-35.

27. Gao Z, Zhang Z, Zhang X, Kulczyk-Malecka J, Liu H, Kelly P, et al. A conformable high temperature nitride coating for Ti alloys. *Acta Mater.* 2020;189:274-83.
28. Nascimento CD, Granemann Souza E, Aguzzoli C. Correlation between electrical and compositional properties in cadmium sulfide deposited by laser ablation. *Thin Solid Films.* 2018;651:39-41.
29. Hernandez-Como N, Martinez-Landeros V, Mejia I, Aguirre-Tostado FS, Nascimento CD, Azevedo GM, et al. Defect control in room temperature deposited cadmium sulfide thin films by pulsed laser deposition. *Thin Solid Films.* 2014;550:665-8.
30. Lang W. *Sensors and measurement systems.* Aalborg: River Publishers; 2019.
31. Wang C, Brault P, Sauvage T. Density measurement of W thin films coating by combination of ion beam analysis and scanning electron microscopy. *Eur Phys J Appl Phys.* 2005;31(1):17-22.
32. Mayer M. SIMNRA, A simulation program for the analysis of NRA, RBS and ERDA. *AIP Conf Proc.* 1999;475:541-4.
33. Dobrzanski LA, Lukaszowicz K, Labisz K. Structure, texture and chemical composition of coatings deposited by PVD techniques. *Arch. Mater. Sci. Eng.* 2009;37(1):45-52.
34. Li J, Li Y, Huang M, Xiang Y, Liao Y. Improvement of aluminum lithium alloy adhesion performance based on sandblasting techniques. *Int J Adhes Adhes.* 2018;84:307-16.
35. Jacobson S, Hogmark S. On the tribological character of boundary lubricated DLC coated components. *Tribol. Ser.* 2002;40:337-45.
36. Sun CC, Lee SC, Hwang WC, Hwang JS, Tang IT, Fu YS. Surface free energy of alloy nitride coatings deposited using closed field unbalanced magnetron sputter ion plating. *Mater Trans.* 2006;47(10):2533-9.
37. Miccoli I, Edler F, Pfnur H, Tegenkamp C. The 100th anniversary of the four-point probe technique: the role of probe geometries in isotropic and anisotropic systems. *J Phys Condens Matter.* 2015;27(22):1-29.
38. Tsai W, Delfino M, Fair JA, Hodul D. Temperature dependence of the electrical resistivity of reactively sputtered TiN films. *J Appl Phys.* 1993;73:4462-7.
39. Pillouda D, Pierson JF, Cavaleiro A, Marco de Lucas MC. Effect of germanium addition on the properties of reactively sputtered ZrN films. *Thin Solid Films.* 2005;492(1-2):180-6.
40. Transmai Equipamentos Médicos Hospitalares Ltda. BP-150 user manual. São Paulo; 2002. Chapter 4, Technical specifications; p. 32.
41. Ikuma Y, Shoji A. High temperature oxidation of ZrN powder in oxygen atmosphere. *Trans Mater Res Soc Jpn.* 1994;1:277-80.
42. Hedberg YS, Wallinder IO. Metal release from stainless steel in biological environments: a review. *Biointerphases.* 2016;11:018901.